Nonlinear dynamic characteristics of a flexible rotor system with local rub-impact

H. Ma[1], **X. Y. Tai**[1], **H. L. Yi**[2], **S. Lv**[1], **B. C. Wen**[1]
[1] School of Mechanical Engineering and Automation, Northeastern University, Shenyang 110819, China
[2] Shenyang Blower Works Group Corporation, Shenyang, 110869, China

E-mail: mahui_2007@163.com

Abstract. In this paper, nonlinear dynamic characteristics of a single span rotor system with two discs are investigated under fixed-point and local arc rub-impact conditions. A twenty-degree-of-freedom model considering the gyroscopic effect is developed, the simple Coulomb friction model and piecewise linear spring model to describe the contact between the rotor and the stator. The vibration chracteristics of the rotor system with two types of rub-impact forms are analyzed with respect to the effects of rotating speed by using spectrum cascades, vibration waveforms, orbits and frequency spectra. The simulation results show that different rotor motions appear, such as P1(period-1), P2, P3 and P4 with the increasing rotating speed under two rub-impact conditions. And some combination frequency components and continuous spectra appear under the local arc rub-impact condition, which are different from those under the fixed-point rub-impact condition.

1. Introduction

Due to the increasing demand for high speed and high efficiency, the clearance between the rotor and stator in rotating machinery is becoming smaller and smaller. As a result, the rub-impact, which refers to the contact between the rotating and non-rotating structures in a machine, has become one of the most common damaging malfunctions in rotating machinery. Many works on different rub-impact forms, such as point, local annular and full annular rub-impacts, have been extensively studied [1].

Many researches on the fixed-point rub-impact have been carried out by Ma et al., Han et al., Lahriri et al., Hu et al. and many others. Ma et al. [2,3] analyzed nonlinear dynamic characteristics of a flexible rotor system with fixed-point rubbing by numerical simulation and experimental verification. Han et al. [4] developed a FE (finite element) model of the rotor system and analyzed different rotor motions caused by rub-impact occurring at fixed limiters. Lahriri et al. [5,6] proposed a new unconventional backup bearing design (similar to four point rubbing device) in order to reduce the rub related severity in friction and center the rotor at impact events. The result shows that the rotor with impacts is forced to the center of the backup bearing and the lateral motion is mitigated. Hu et al. [7] analyzed the features of sharp rubbing between the rotor and stator in a rotor system by experiments. Their results show that in the early rubbing stage, there are the sub-harmonics vibration of the order 1/3 and 2/3 obviously.

[1] Corresponding author (H. Ma). Tel.: +86 24 83684491; fax: +86 24 83679731.

Many efforts have been devoted to study the local rubbing fault, such as Muszynska et al., Abuzaid et al., Chu et al., and Roques et al. Muszynska et al. [8] discussed chaotic response of unbalance rotor-bearing-stator systems with local rubbing. The results show that at low rotational speeds, the rotor's response exhibits 1*X* (*X* denotes rotating frequency) vibration as the lowest frequency component. At a speed roughly equal to twice the rotor's first lateral natural frequency, a 1*X*/2 sub-synchronous vibration component appears, and continuous until the rotational speed reaches 3 times the rotor's first natural frequency. Then, the 1*X*/2 is replaced by 1*X*/3 vibration as the lowest frequency component. Abuzaid et al. [9] investigated the effect of partial rotor-stator rubbing both experimentally and analytically. The results show that the features of light rubbing include 1*X*, 2*X* and 3*X*, whereas severe rubbing include 1*X*/3 and 2*X*/3. Chu et al. [10] studied the nonlinear vibration of a rub-impact rotor system and observed a variety of periodic and chaotic vibrations. The experiments show that the system motion generally contains multiple harmonic components, such as 2*X*, 3*X*, and 1/2-based fractional harmonic components, such as 1*X*/2 and 3*X*/2. Under some special conditions, the 1/3-based fractional harmonic components can also be observed. Roques et al. [11] presented a rotor-stator model of a turbogenerator and investigated rotor-stator rubbing caused by an accidental blade-off imbalance. Thereinto, the rotor system is modeled using FE method, rotor-stator rubbing is simulated using node-to-line contact and the highly nonlinear equations due to contact conditions are solved through an explicit prediction-correction time-marching procedure combined with the Lagrange multiplier approach.

Aiming at full annular rubbing, Dai et al. [12,13] adopted the simple Coulomb friction model and piecewise linear spring model to describe the contact between the rotor and the stationary stop, established the dynamic equations of the rotor that does precession roughly enough to rub with the displacement stop in the support and analyzed nonlinear vibration responses in the process of rubbing by numerical simulation. Choi [14] investigated the whirling motion of the rotor with full annular rub. His study shows that the effects of the friction coefficient and the eccentricity of the rotor can explain the onset of backward rolling and backward slipping as the rotor speed increases or decreases. Jiang et al. [15] analyzed the stability of the full annular rub solutions of a modified Jeffcott rotor with a given rotor-stator clearance and cross-coupling influences. Adopting a linear spring model to model the local impact-deformation phenomenon, Xu et al. [16] studied the synchronous full annular rub motion of a Jeffcott rotor and its dynamic stability behaviour in detail.

From experiments on aero-engine test rigs, it has been observed that rubbings often only occur at fixed points or local arc area along the radial direction if they are caused by the deformation of compressor cases [17], which is called fixed-point or local arc rub-impact in this paper. In our study, a twenty-degree-of-freedom model of a flexible rotor system considering the gyroscopic effect is established. Vibration responses are simulated under fixed-point and local arc rub-impact conditions. The results will give deep insight into the local rub-impact mechanism.

2. Fixed-point and local arc rub-impact models

Fixed-pint rub-impact is that the rotor contacts a fixed point of the stator once in one cycle, which usually occurs when the stator stiffness is greater than that of the rotor system or bumps caused by the stator deformation appear. Schematic diagram of the fixed-point rub-impact is shown in figure 1(a). In the figure, ω is rotating speed, F_{rx} and F_{ry} are normal and tangential rub-impact forces respectively and their expressions are as follows

$$\begin{cases} F_{rx} = -k_r(x-c)H(x-c) \\ F_{ry} = f_r F_{rx} = -f_r k_r(x-c)H(x-c) \end{cases}, \tag{1}$$

where c is an initial clearance between the rotor and the stator, k_r is the stator stiffness in the rub-impact direction, f_r is friction coefficient at rub-impact position, H is Heaviside function and its expression can be written as

$$H(x-c)=\begin{cases}0 & \text{if } x<c\\ 1 & \text{if } x\geq c\end{cases}.$$

Schematic diagram of the local arc rub-impact is shown in figure 1(b). In the figure, o is the center of the stator, o' is the center of the rotor, β is the angle between oo' and the positive x-axis, α_0 and α_1 are start and end angles between the stator and the positive x-axis, F_n and F_t are normal and tangential rub-impact forces respectively and their expressions are as follows

$$\begin{cases}F_n=(r-c)k_r\\ F_t=f_rF_n\end{cases}\quad (r\geq c \text{ and } \alpha_0\leq\beta\leq\alpha_1), \tag{2}$$

where $r=\sqrt{x^2+y^2}$ is the radial displacement of the rotor. The component forces F_{rx} and F_{ry} of rub-impact force in x and y directions can be expressed as follows

$$\begin{Bmatrix}F_{rx}\\ F_{ry}\end{Bmatrix}=-H(r-c)\frac{(r-c)k_r}{r}\begin{pmatrix}1 & -f_r\\ f_r & 1\end{pmatrix}\begin{Bmatrix}x\\ y\end{Bmatrix}\quad (\alpha_0\leq\beta\leq\alpha_1), \tag{3}$$

where $H(r-c)=\begin{cases}0 & \text{if } r<c\\ 1 & \text{if } r\geq c\end{cases}$.

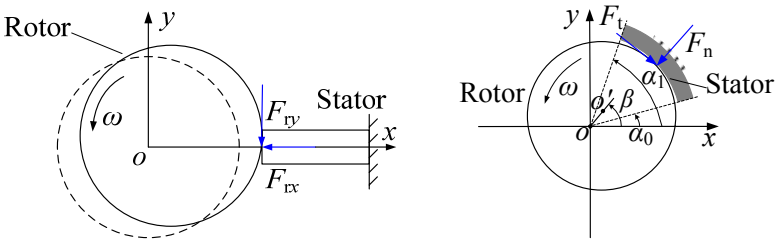

(a) fixed-point rub-impact (b) local arc rub-impact

Figure 1. Schematic diagrams of fixed-point and local arc rub-impacts

3. The motion differential equations of the rotor system with rub-impact

In order to study the rub-impact fault efficiently, a mathematical model of the rotor-bearing system, which is depicted in Fig. 1, is simplified according to the following assumptions.

(a) The movements of the rotor in torsional and axial directions are negligible; the journals, coupling and discs are simulated by five lumped mass points and the corresponding points are connected by massless shaft sections of lateral stiffness; each point has four degrees of freedom including two rotation and two translation freedom, in which m_i (i=1,2,3,4,5) are lumped masses.

(b) The bearings are modelled ideally by linear stiffness and damping, where k_{blx}, k_{bly}, c_{blx}, c_{bly} and k_{brx}, k_{bry}, c_{brx}, c_{bry} are stiffnesses and dampings of the left and right bearings in x and y directions, respectively.

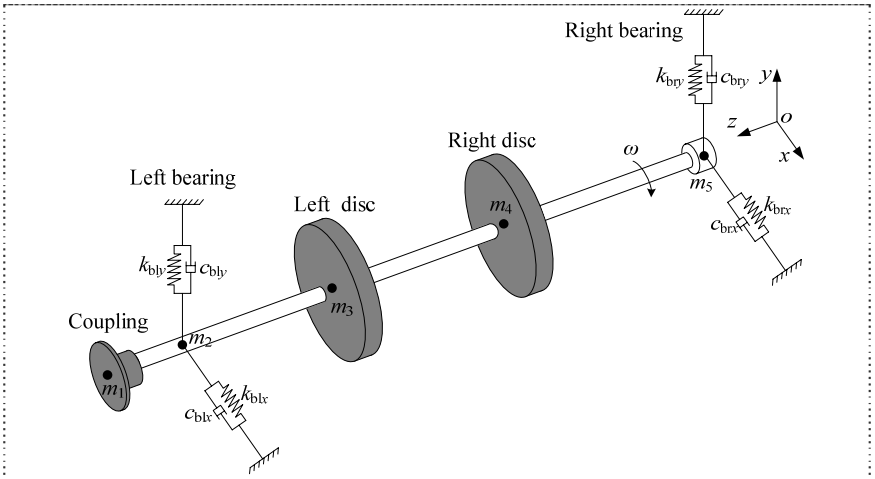

Figure 2. Schematic diagram of a rotor system

Assuming that rub-impact occurs at the left disc and the motion differential equations of the rotor-bearing system with twenty degrees of freedom can be deduced as

$$\boldsymbol{M}\ddot{\boldsymbol{q}} + (\boldsymbol{G} + \boldsymbol{C})\dot{\boldsymbol{q}} + \boldsymbol{K}\boldsymbol{q} = \boldsymbol{F}_{\mathrm{u}} + \boldsymbol{F}_{\mathrm{r}}, \tag{4}$$

$$\boldsymbol{M} = \begin{bmatrix} \boldsymbol{M}_x & 0 \\ 0 & \boldsymbol{M}_y \end{bmatrix},\ \boldsymbol{M}_x = \boldsymbol{M}_y = \mathrm{diag}[m_1, J_{\mathrm{d}1}, m_2, J_{\mathrm{d}2}, m_3, J_{\mathrm{d}3}, m_4, J_{\mathrm{d}4}, m_5, J_{\mathrm{d}5}], \tag{5}$$

$$\boldsymbol{G} = \omega\boldsymbol{J} = \omega\begin{bmatrix} 0 & \boldsymbol{J}_1 \\ -\boldsymbol{J}_1^{\mathrm{T}} & 0 \end{bmatrix},\ \boldsymbol{J}_1 = \mathrm{diag}[0, J_{\mathrm{p}1}, 0, J_{\mathrm{p}2}, 0, J_{\mathrm{p}3}, 0, J_{\mathrm{p}4}, 0, J_{\mathrm{p}5}], \tag{6}$$

where $J_{\mathrm{p}i}$ and $J_{\mathrm{d}i}$ (i=1,2…5) are the polar moment of inertia and the diametral moment of inertia of lumped points, respectively.

$$\boldsymbol{K} = \begin{bmatrix} \boldsymbol{K}_x & 0 \\ 0 & \boldsymbol{K}_y \end{bmatrix}, \tag{7}$$

$$\boldsymbol{K}_x = \begin{bmatrix} k_{11} & k_{12} & k_{13} & k_{14} & 0 & 0 & 0 & 0 & 0 & 0 \\ k_{12} & k_{22} & k_{23} & k_{24} & 0 & 0 & 0 & 0 & 0 & 0 \\ k_{13} & k_{23} & k_{33}+k_{\mathrm{blx}} & k_{34} & k_{35} & k_{36} & 0 & 0 & 0 & 0 \\ k_{14} & k_{24} & k_{34} & k_{44} & k_{45} & k_{46} & 0 & 0 & 0 & 0 \\ 0 & 0 & k_{35} & k_{45} & k_{55} & k_{56} & k_{57} & k_{58} & 0 & 0 \\ 0 & 0 & k_{36} & k_{46} & k_{56} & k_{66} & k_{67} & k_{68} & 0 & 0 \\ 0 & 0 & 0 & 0 & k_{57} & k_{67} & k_{77} & k_{78} & k_{79} & k_{7,10} \\ 0 & 0 & 0 & 0 & k_{58} & k_{68} & k_{78} & k_{88} & k_{89} & k_{8,10} \\ 0 & 0 & 0 & 0 & 0 & 0 & k_{79} & k_{89} & k_{99}+k_{\mathrm{brx}} & k_{9,10} \\ 0 & 0 & 0 & 0 & 0 & 0 & k_{7,10} & k_{8,10} & k_{9,10} & k_{10,10} \end{bmatrix}, \tag{8}$$

$$\boldsymbol{K}_y=\begin{bmatrix} k_{11} & -k_{12} & k_{13} & -k_{14} & 0 & 0 & 0 & 0 & 0 & 0 \\ -k_{12} & k_{22} & -k_{23} & k_{24} & 0 & 0 & 0 & 0 & 0 & 0 \\ k_{13} & -k_{23} & k_{33}+k_{\mathrm{bly}} & -k_{34} & k_{35} & -k_{36} & 0 & 0 & 0 & 0 \\ -k_{14} & k_{24} & -k_{34} & k_{44} & -k_{45} & k_{46} & 0 & 0 & 0 & 0 \\ 0 & 0 & k_{35} & -k_{45} & k_{55} & -k_{56} & k_{57} & -k_{58} & 0 & 0 \\ 0 & 0 & -k_{36} & k_{46} & -k_{56} & k_{66} & -k_{67} & k_{68} & 0 & 0 \\ 0 & 0 & 0 & 0 & k_{57} & -k_{67} & k_{77} & -k_{78} & k_{79} & -k_{7,10} \\ 0 & 0 & 0 & 0 & -k_{58} & k_{68} & -k_{78} & k_{88} & -k_{89} & k_{8,10} \\ 0 & 0 & 0 & 0 & 0 & 0 & k_{79} & -k_{89} & k_{99}+k_{\mathrm{bry}} & -k_{9,10} \\ 0 & 0 & 0 & 0 & 0 & 0 & -k_{7,10} & k_{8,10} & -k_{9,10} & k_{10,10} \end{bmatrix}. \quad (9)$$

The matrix elements of $\boldsymbol{K}_x$ and $\boldsymbol{K}_y$ are calculated as follows:

$$\begin{cases} k_{11}=a_{11} \\ k_{12}=a_{21} \\ k_{13}=-a_{11} \\ k_{14}=a_{21} \end{cases}, \begin{cases} k_{22}=l_1a_{21}-a_{31} \\ k_{23}=-a_{21} \\ k_{24}=a_{31} \end{cases}, \begin{cases} k_{33}=a_{11}+a_{12} \\ k_{34}=-a_{21}+a_{22} \\ k_{35}=-a_{12} \\ k_{36}=a_{22} \end{cases}, \begin{cases} k_{44}=l_1a_{21}-a_{31}+l_2a_{22}-a_{32} \\ k_{45}=-a_{22} \\ k_{46}=a_{32} \end{cases}, \begin{cases} k_{55}=a_{12}+a_{13} \\ k_{56}=-a_{22}+a_{23} \\ k_{57}=-a_{13} \\ k_{58}=a_{23} \end{cases},$$

$$\begin{cases} k_{66}=l_2a_{22}-a_{32}+l_3a_{23}-a_{33} \\ k_{67}=-a_{23} \\ k_{68}=a_{33} \end{cases}, \begin{cases} k_{77}=a_{13}+a_{14} \\ k_{78}=-a_{23}+a_{24} \\ k_{79}=-a_{14} \\ k_{7,10}=a_{24} \end{cases}, \begin{cases} k_{88}=l_3a_{23}-a_{33}+l_4a_{24}-a_{34} \\ k_{89}=-a_{24} \\ k_{8,10}=a_{34} \end{cases}, \begin{cases} k_{99}=a_{14} \\ k_{9,10}=-a_{24} \\ k_{10,10}=l_4a_{24}-a_{34} \end{cases},$$

and

$$\begin{cases} a_{1i}=\dfrac{12EI}{l_i^3} \\ a_{2i}=\dfrac{1}{2}l_ia_{1i}, i=1,2,3,4, \\ a_{3i}=\dfrac{1}{6}l_i^2a_{1i} \end{cases} \quad (10)$$

in which E, l_i and I are the Young's modulus of elasticity, the distance between every two consecutive lumped mass points and the area moment of inertia respectively.

$$\boldsymbol{C}=\boldsymbol{C}_1+\boldsymbol{C}_2, \quad (11)$$

$$\boldsymbol{C}_1=\alpha\boldsymbol{M}+\beta\boldsymbol{K}, \quad (12)$$

$$\alpha=\frac{60(\omega_{\mathrm{n}2}\xi_1-\omega_{\mathrm{n}1}\xi_2)\omega_{\mathrm{n}1}\omega_{\mathrm{n}2}}{\pi(\omega_{\mathrm{n}2}^2-\omega_{\mathrm{n}1}^2)}, \beta=\frac{\pi(\omega_{\mathrm{n}2}\xi_2-\omega_{\mathrm{n}1}\xi_1)}{15(\omega_{\mathrm{n}2}^2-\omega_{\mathrm{n}1}^2)}, \quad (13)$$

where $\omega_{\mathrm{n}1}$ and $\omega_{\mathrm{n}2}$ are the first and second order natural frequencies (r/min); ξ_1 and ξ_2 refer to the first and second order modal damping ratios, respectively.

$$\boldsymbol{C}_2=\mathrm{diag}[0,0,c_{\mathrm{blx}},0,0,0,0,0,0,0,0,c_{\mathrm{bly}},0,0,0,0,0,0,0] \quad (14)$$

$$\boldsymbol{q}=[x_1,\theta_{y1},x_2,\theta_{y2},x_3,\theta_{y3},x_4,\theta_{y4},x_5,\theta_{y5},y_1,\theta_{x1},y_2,\theta_{x2},y_3,\theta_{x3},y_4,\theta_{x4},y_5,\theta_{x5}]^{\mathrm{T}}, \quad (15)$$

where x_i, y_i, θ_{xi} and θ_{yi} (i=1,2,3,4,5) are the displacements in x and y directions and angles of orientation associated with the x and y axes, respectively.

$$\begin{aligned}\boldsymbol{F}_{\mathrm{u}} = [&0,0,0,0,m_3e\omega^2\cos(\omega t+\varphi_1),0,m_4e\omega^2\cos(\omega t+\varphi_2),0,0,0,\\ &0,0,0,0,m_3e\omega^2\sin(\omega t+\varphi_1),0,m_4e\omega^2\sin(\omega t+\varphi_2),0,0,0]^{\mathrm{T}},\end{aligned} \tag{16}$$

where m_3e, m_4e, φ_1 and φ_2 denote the eccentricity of unbalance mass of the left and right discs, the initial phase angles of eccentricity in left and right discs, respectively.

$$\boldsymbol{F}_{\mathrm{r}} = \left[0,0,0,0,F_{\mathrm{rx}},0,0,0,0,0,0,0,0,0,F_{\mathrm{ry}},0,0,0,0,0\right]^{\mathrm{T}} \tag{17}$$

in which F_{rx} and F_{ry} are rub-impact forces of the left disc in x and y directions.

The model parameters of the rotor and the bearing are listed in Table 1. The first and second natural frequencies can be determined to be about 27.27 Hz and 98.48 Hz. Eq. (4) is solved by using numerical methods and Newmark-β integration method is adopted because it is a kind of robust algorithm for solving nonlinear equations in the time domain. In this paper, the spectrum cascade is used to exhibit continuous changes of the frequency components of the rotor-bearing system, rotor orbit is used to show the axis trace moving direction and vibration waveform to indicate time domain features under some rotating speeds.

Table 1. Model parameters of the rotor-bearing system

m_1,m_2,m_3,m_4,m_5 (kg)	0.0439, 0, 0.741, 0.741, 0
J_{p1},J_{d1} (kg·m^2)	2.42×10^{-6}, 2.56×10^{-6}
J_{p2},J_{d2}(kg·m^2)	0, 0
J_{p3},J_{d3}(kg·m^2)	4.09×10^{-4}, 2.4×10^{-4}
J_{p4},J_{d4}(kg·m^2)	4.09×10^{-4}, 2.4×10^{-4}
J_{p5},J_{d5}(kg·m^2)	0, 0
k_{blx},k_{bly},k_{brx},k_{bry} (N/m)	1×10^5,2×10^5,2×10^8,5×10^8
c_{blx},c_{bly},c_{brx},c_{bry} (N·s/m)	100,200,1000,2000
ξ_1 , ξ_2	0.02, 0.04
m_3e, m_4e (kg·m)	1.56×10^{-4}
φ_1, φ_2(rad)	0, 0

4. Numerical simulation of fixed-point and local arc rub-impacts

4.1. Fixed-point rub-impact simulation

Material parameters of rotor are as follows: Young's modulus of elasticity E=207 GPa, Poisson ratio υ=0.3. The stator stiffness k_{r}=8 MN/m and the clearance between the rotor and the stator c=0.1 mm, friction coefficient f_{r}=0.3. Spectrum cascade of the system with rotating speed is shown in figure 3. In the figure 1X denotes rotating frequency.

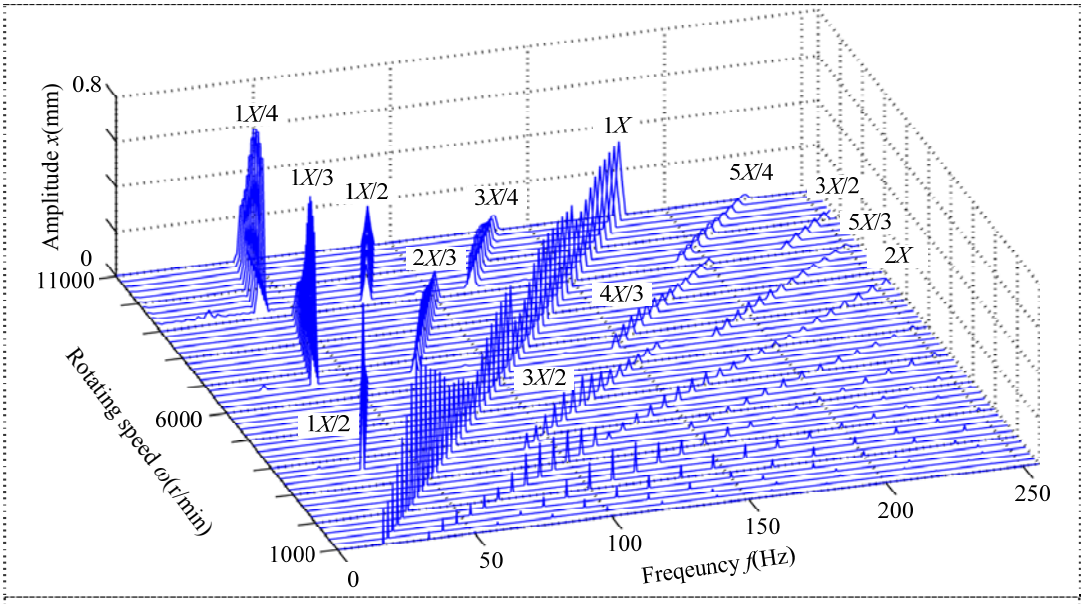

Figure 3. Spectrum cascade of the left disc with fixed-point rub-impact

From figure 3 it can be seen that the frequency feature includes 1*X*, 2*X* in the range of $\omega \in [1000, 3500]$ r/min, which show system motion is P1 (period-1); 1/2 fractional harmonic components, such as 1*X*/2, 3*X*/2, 5*X*/2, etc., in the range of $\omega \in [3500, 6300]$ r/min; 1/3 fractional harmonic components in the range of $\omega \in [6300, 9200]$ r/min; 1/4 fractional harmonic components in the range of $\omega \in [9200, 10000]$ r/min. The detailed vibration responses at ω=1000, 5000, 8500 r/min are shown in Fig. 4, which shows, from the left to the right, vibration waveforms, orbits and spectra. In the orbits, the black line denotes the orbits without rub-impact and red line the orbits with rub-impact.

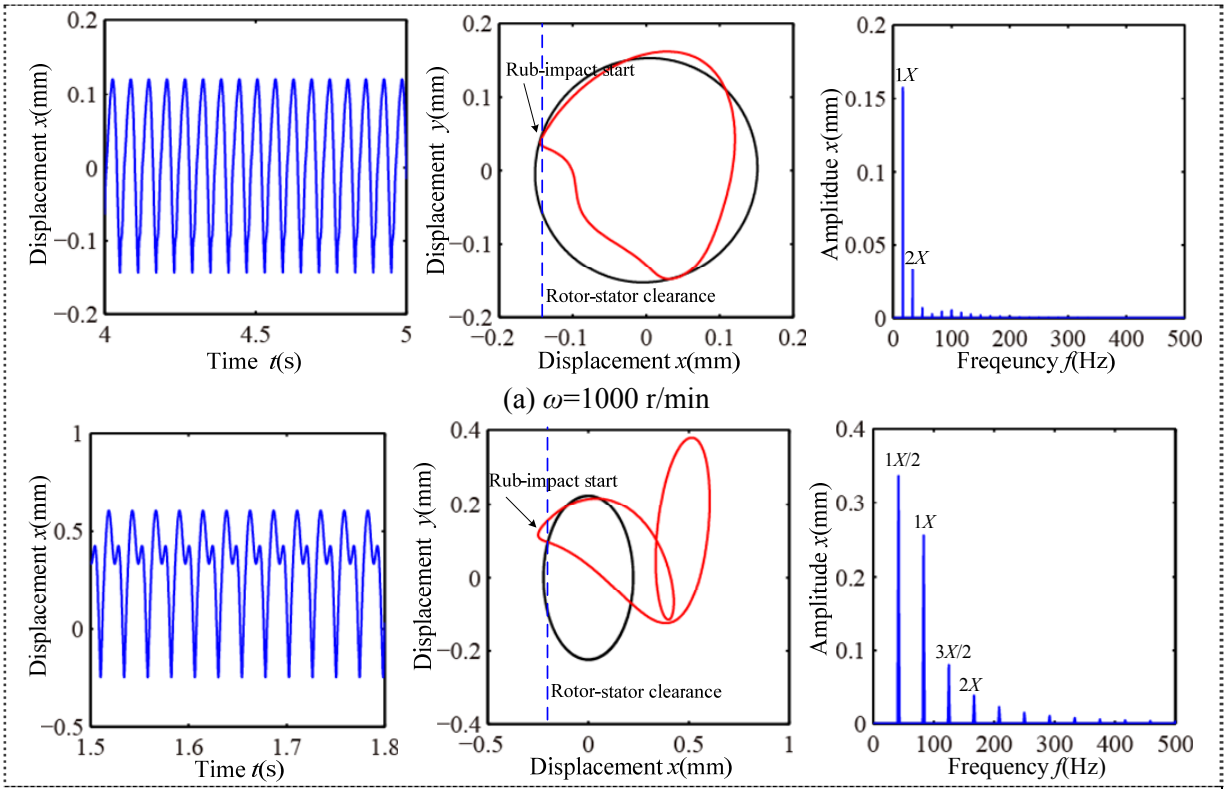

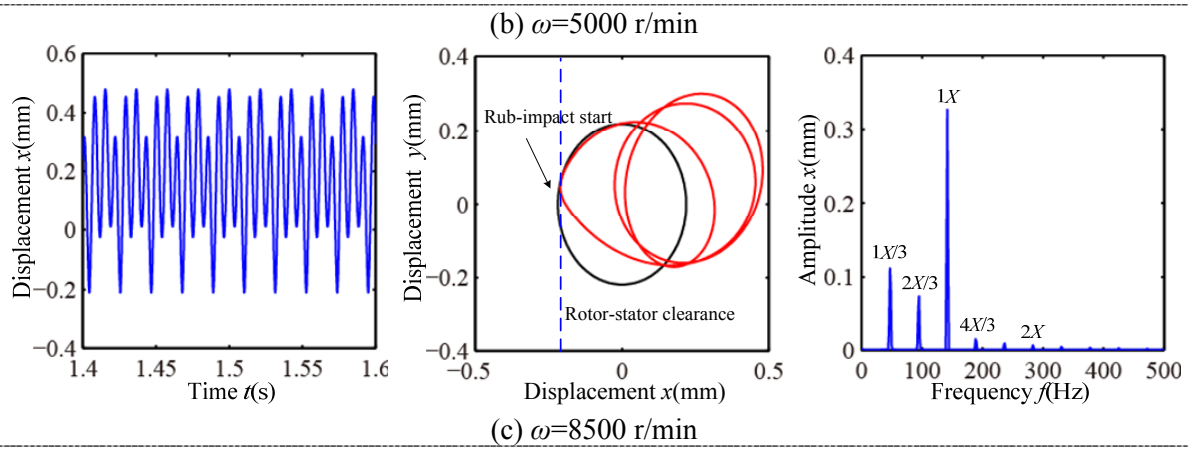

Figure 4. Vibration response of the system at ω=1000,5000, 8500 r/min

4.2. Local arc rub-impact simulation

The clearance between the rotor and the stator c=0.14 mm and rub-impact regional angle $\alpha=\alpha_1-\alpha_0$= 30º and other parameters are the same as those in section 4.1. Spectrum cascade of the system with rotating speed is shown in figure 5. As a whole, the system motions (P1, P2, P3 and P4) with local arc rub-impact are similar to those under fixed-point rub-impact condition. However frequency features of the former, especially the transition regions between different motions, are more complicated than those of the latter. Some continuous spectra appear in the ranges of $\omega\in$[1800,2000], [3000,3800], [5000,6000] and [8800,9200] r/min, which show the complexity of the local arc rub-impact.

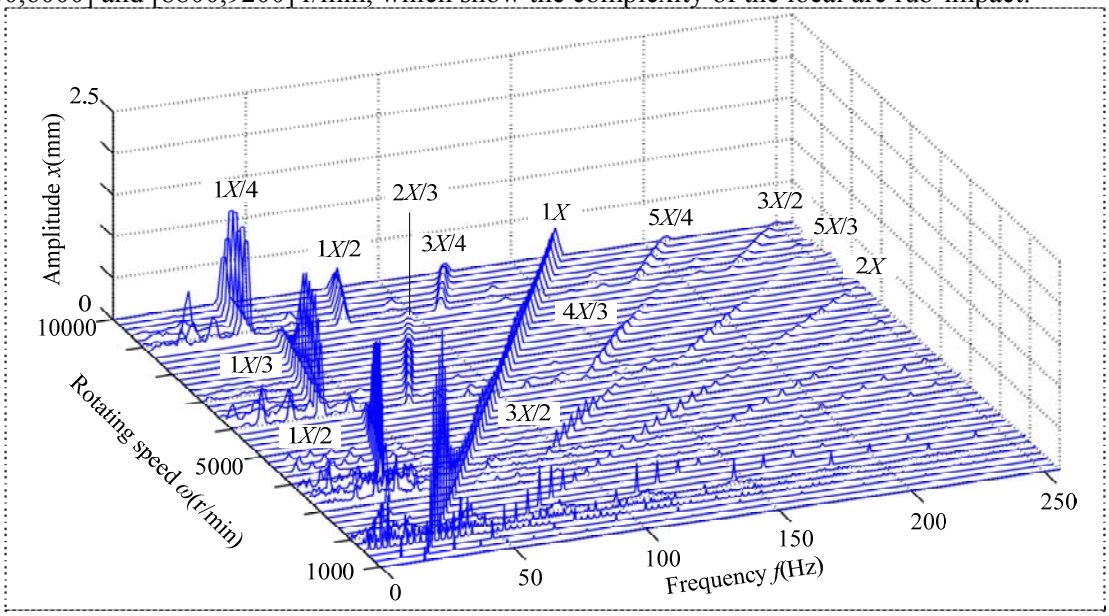

Figure 5. Spectrum cascade of the left disc with local arc rub-impact

The detailed vibration responses at ω=2000, 4000, 6000 r/min are shown in Fig. 6. Combination frequency components appear and the system motion is quasi-periodic at ω=2000 r/min. 1/2 fractional harmonic components, such as 1X/2, 3X/2, appear at ω=4000 r/min, which show system motion is P2. Low frequency components with big amplitudes and continuous spectra appear at ω=6000 r/min.

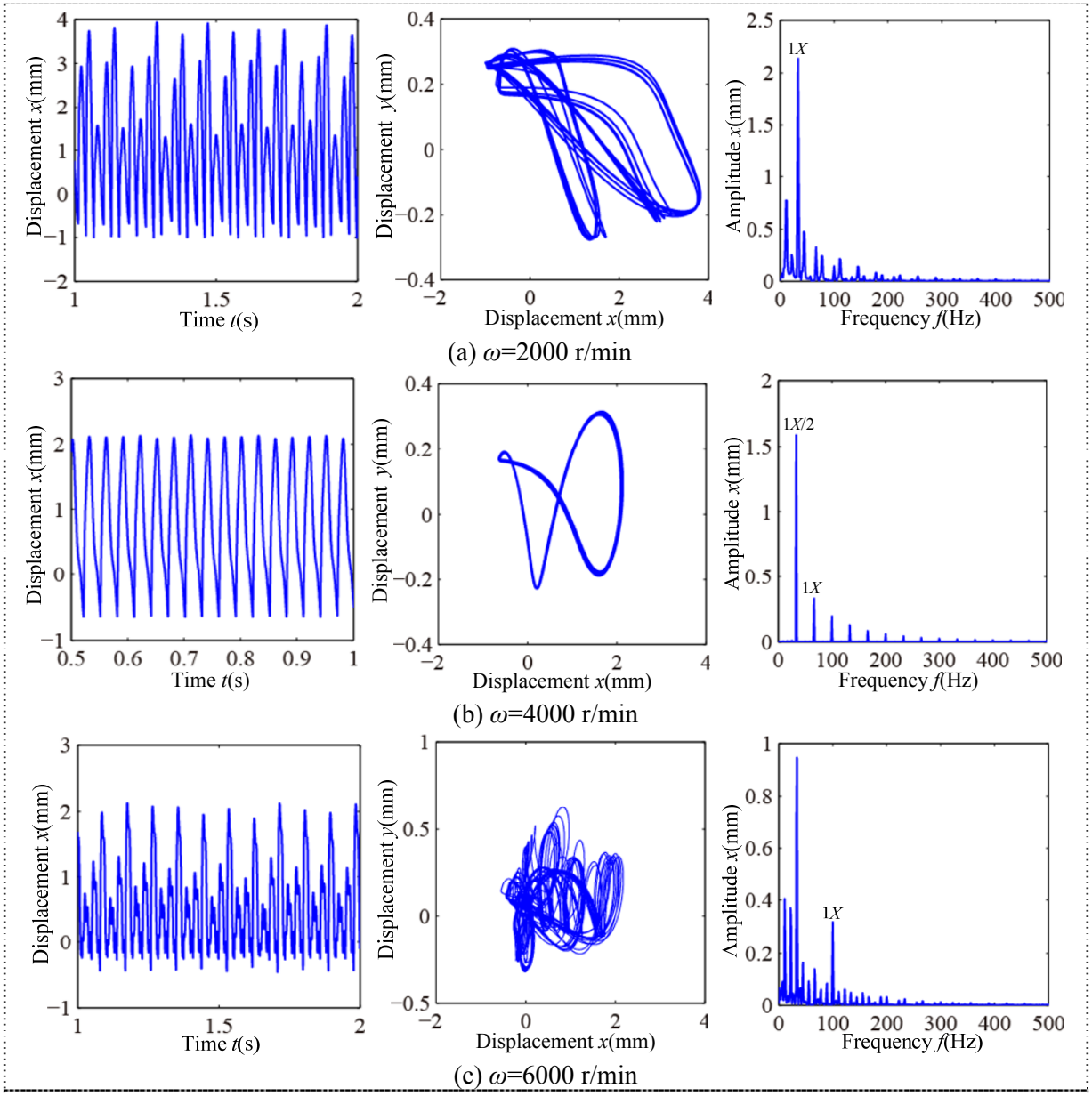

Figure 6. Vibration response of the system at ω=2000,4000, 6000 r/min

5. Conclusions

In this paper, a twenty-degree-of-freedom model of a flexible rotor system considering the gyroscopic effect is developed. The system vibration responses are analyzed under the fixed-point and local arc rub-impact conditions by numerical simulation. Some conclusions drawn from the study can be summarized as follows.

Under the fixed-point rub-impact condition, system motion is from period-1 through period-2 and period-3 to period-4 with the increase of the rotating speed. On the whole, the motion forms under the local rub-impact condition are similar to those under the fixed-point rub-impact, however, some combination frequency components and continuous spectra appear at the transition regions between different motions. These features show that the local rub-impact is more complicated than fixed-point rub-impact.

Acknowledgments

We are grateful to the China Natural Science Funds (NSFC, Grant No. 50805019), the Fundamental Research Funds for the Central Universities (Grant No. N100403008) and the Program for New Century Excellent Talents in University (Grant No. NCET-11-0078) for providing financial support for this work.

References

[1] Wen B C, Wu X H, Ding Q and Han Q K 2004 *Theory and experiment of nonlinear dynamics for rotating machinery with faults* (Beijing: Science Press)
[2] Ma H, Tai X Y, Sun J and Wen B C 2001 Analysis of dynamic characteristics for a dual-disk rotor system with single rub-impact *Advanced Science Letters* **4** 2782-89
[3] Ma H, Shi C Y, Han Q K and Wen B C 2012 Fixed-point rubbing fault characteristic analysis of a rotor system based on contact theory *Mech Syst Signal Pr Preprint* j.ymssp.2012.10.009
[4] Han Q K, Zhang Z W, Wen B C 2008 Periodic motions of a dual-disc rotor system with rub-impact at fixed limiter *P I Mech Eng C-J Mec* **222** 1935-46.
[5] Lahriri S, Weber H I, Santos I F, et al. 2012 Rotor-stator contact dynamics using a non-ideal drive-Theoretical and experimental aspects *J Sound Vib* **331** 4518-36.
[6] Lahriri S, Santos I F, Weber H I, et al. 2012 On the nonlinear dynamics of two types of backup bearings-theoretical and experimental aspects. *J Eng Gas Turb Power* **134** 112503-1-13.
[7] Hu N Q, Zhang Y, Liu Y Z, et al. 2002 Experimental research on vibration characteristics of sharp rub-impact between rotor and stator of a rotor system *China Mechanical Engineering* **13** 777-9
[8] Muszynaka A, Goldman P 1995 Chaotic responses of unbalanced rotor/bearing/stator system with looseness or rubs *Chaos Soliton Fract* **5** 1683-1704
[9] Abuzaid M A, Eleshaky M E, Zedan M G 2009 Effect of partial rotor-to-stator rub on shaft vibration *J Mech Sci Technol* **23** 170-182
[10] Chu F L, Lu W X 2005 Experimental observation of nonlinear vibrations in a rub–impact rotor system *J Sound Vib* **283** 621-643
[11] Roques S, Legrand M, Cartraud P, et al. 2010 Modeling of a rotor speed transient response with radial rubbing *J Sound Vib* **329** 527-546
[12] Dai X, Zhang X, Jin X 2001 The partial and full rubbing of a flywheel rotor-bearing-stop system *International Journal of Mechanical Sciences* **43** 505-519
[13] Dai X, Jin Z, Zhang X 2002 Dynamic behavior of the full rotor/stop rubbing: numerical simulation and experimental verification *J Sound Vib* **251** 807-822
[14] Choi Y S 2002 Investigation on the whirling motion of full annular rotor rub *J Sound Vib* **258** 191-198.
[15] Jiang J, Ulbrich H 2001 Stability analysis of sliding whirl in a nonlinear Jeffcott rotor with cross coupling stiffness coefficients *Nonlinear Dynamics* **24** 269-283
[16] Xu b, Xu W N, Zhang W 2006 Study of synchronous full annular rub of Jeffcott rotor and its dynamic stability *Journal of Fudan University* (*Natural Science*) **45** 148-154.
[17] Wang D Y 1995 Research and extract of vibration features on rubbing between rotor and stator for aeroengine PhD Thesis (Beijing: University of Aeronautics and Astronautics)